Unravelling a complex catalyst deactivation in which selectivity affects conversion oxygen-assisted styrene synthesis at industrially-relevant conditions

Melián-Cabrera, Ignacio; Zarubina, Valeriya; Jansma, Harrie

DOI
10.1016/j.cej.2024.152348

Publication date
2024

Document Version
Final published version

Published in
Chemical Engineering Journal

Chemical Engineering Journal 494 (2024) 152348

Contents lists available at ScienceDirect

Chemical Engineering Journal

journal homepage: www.elsevier.com/locate/cej

Unravelling a complex catalyst deactivation in which selectivity affects conversion: oxygen-assisted styrene synthesis at industrially-relevant conditions

Ignacio Melián-Cabrera [a,b,*], Valeriya Zarubina [b,c], Harrie Jansma [d]

[a] Applied Photochemistry and Materials for Energy Group, University of La Laguna, Avda. Astrofísico Francisco Sánchez, s/n, PO BOX 456, 38200 San Cristóbal de La Laguna, S/C de Tenerife, Spain
[b] Faculty of Science and Engineering, University of Groningen, Nijenborgh 4, Nijenborgh 4, 9747 AG Groningen, The Netherlands
[c] Erasmus University Rotterdam, Erasmus University College (EUC), Nieuwemarkt 1A, 3011 HP Rotterdam, The Netherlands
[d] Catalysis Engineering, Chemical Engineering Department, Faculty of Applied Sciences, Delft University of Technology, Van der Maasweg 9, 2629 HZ Delft, The Netherlands

ARTICLE INFO

To Prof. Bárbara T. García Pawelec, ad honorem senior scientist at the Spanish National Research Council.

Keywords:
Oxidative dehydrogenations
Styrene synthesis
Novel deactivation mechanism
Catalyst stability
Active coke
Selectivity-induced conversion model

ABSTRACT

The oxidative dehydrogenation of ethylbenzene (EB) into styrene (ST) has been proposed as an alternative to the conventional energy-consuming synthesis of styrene. Various types of catalysts have been reported as promising for the reaction under industrially-relevant conditions. However, they show a complex deactivation behaviour. The EB conversion and the ST selectivity decay, with an increased CO_x selectivity. This phenomenon was investigated by means of experimental data and reaction model analysis, using two reference inorganic catalysts. The active catalyst is the deposited coke (ODH-coke) and not directly the inorganic material. The coke is formed in the initial reaction phase and promoted by the Lewis acid sites of the inorganic material. The reaction shows an activation period in which the ODH-coke is deposited and the EB conversion reaches a maximum where O_2 is fully converted. From that point onwards, the reaction model is applicable and the experimental data fit very well with low standard deviations. The model explains that the EB conversion's decay with time on stream is associated to changes in the selectivity. Hence, EB conversion is not an independent parameter. This simplifies the understanding of this complex deactivation; the deactivating parameter is the selectivity. At this moment, we cannot discriminate between increased CO_x and decreased ST, or both effects, because both routes are competitive. This case represents a new type of catalyst deactivation behaviour, in which selectivity affects conversion.

1. Introduction

Catalyst stability is one of the most important features for industrial implementation [1,2]. It is desirable to have a stable catalyst under operation for years. Or alternatively, to understand its deactivation so the catalyst reactivation can be integrated in the process [1]. Mechanisms of heterogenous catalyst's deactivation have been well documented for many materials and reactions [1,3–6]. The scope of this work is a reaction of industrial interest, the oxidative dehydrogenation of ethylbenzene to styrene (EB-ODH), whose deactivation shows novel insights.

Styrene is an important basic chemical of the petrochemical sector with broad applications and large production [7]. Its industrial manufacture has several challenges, i.e., equilibrium limitations, low conversion per pass and high energy consumption. To overcome these challenges, the reaction can be carried out with an oxidant and O_2 is effective for this [8,9]. It breaks the equilibrium and this makes the conversion per pass higher and the reaction changes from endothermal to exothermal. This reaction has attracted sustained study in academia and various types of active/selective catalysts have been reported. These types include carbons (containing ketonic active sites) [9–19], inorganic materials that are able to produce active coke [9,14,20–25] and other types [26,27]. Carbons can achieve very high selectivity but their downside is the low thermal stability during a reactivation, though some

* Corresponding author at: Applied Photochemistry and Materials for Energy Group, University of La Laguna, Avda. Astrofísico Francisco Sánchez, s/n, PO BOX 456, 38200 San Cristóbal de La Laguna, S/C de Tenerife, Spain.
E-mail address: Ignacio.melian.cabrera@ull.edu.es (I. Melián-Cabrera).

https://doi.org/10.1016/j.cej.2024.152348
Received 8 February 2024; Received in revised form 19 April 2024; Accepted 16 May 2024
Available online 18 May 2024

progress has been achieved [18].

For inorganic-based catalysts, such as aluminas [20–23] and P_2O_5-containing materials [14,22] under industrially-relevant reaction conditions, the active catalytic phase is the formed coke (ODH-coke) that is deposited onto the inorganic material's surface at the start of the reaction. This phenomenon is attributed to the Lewis acidity of the inorganic support, as proven for aluminas [9,20] (containing Lewis acid sites and no Brønsted sites) and the same is expected for other acidic supports [9]. Specifically, ketonic groups (C=O) on the ODH-coke's surface are considered to be the active sites [28], in a similar manner as proven in carbons [16]. Fig. 1a summarises the reaction pathways in which the ODH-coke is formed either by EB, ST or both. The ODH-coke acts as catalyst for styrene synthesis and is also the precursor for the CO_x formation. The styrene synthesis is a redox process catalysed by C=O groups present on the ODH-coke (Fig. 1b). Scarce information is available in the literature about the CO_x route to be able to answer whether it is a catalysed or non-catalysed process. From our experience, higher partial pressure in O_2 favours the CO_x route [13,14,20–24,28]. Strictly speaking, the inorganic material containing the Lewis acid sites that promotes the formation of ODH-coke is a pre-catalyst. In this work, it is labelled as catalyst for simplicity.

Under industrially-relevant reaction conditions, the stability over time on stream of promising inorganic-based catalysts remains unclear. A pronounced decay of the ethylbenzene (EB) conversion has been observed alongside a drop in styrene selectivity and a raise of the undesired CO_x selectivity, both for alumina and P_2O_5/silica [20,22]. Understanding this topic is crucial for their improved design and implementation. It is important to remark that industrially-relevant reaction conditions involve a high EB concentration and limited O_2; this implies that O_2 should be fully consumed in the reactor due to the various reactions. This is important because unreacted O_2 would provoke explosive conditions in the distillation columns in an industrial setting. However, literature mainly presents examples working at high O_2/EB ratios for this reaction; conditions which are not industrially applicable.

To unravel the above-described complex problem, we have considered here to study the stability in more detail. As catalyst, we initially considered a mesostructured aluminosilicate denoted as MSU, which has wide pores and Lewis acidity to promote the active ODH-coke. Subsequently, the study was expanded with a more styrene-selective catalyst based on P_2O_5/silica. From the results, a novel deactivation mechanism has been identified, where conversion and selectivity are linked. Thus, rather than two parameters being affected in the deactivation, solely selectivity governs the deactivation.

2. Methods

2.1. Materials

The mesoporous Al-MSU-F was purchased from Sigma Aldrich (code: 643629); it is denoted along the manuscript as MSU for simplicity. The as-received powdery MSU was pelletised at mild pressure to avoid mechanically-induced damage and sieved into the 212–425 μm fraction. The Si/Al atomic ratio as determined by elemental analysis was ca. 47. Mesoporous amorphous silica extrudates was kindly supplied by Saint-Gobain NorPro (code: 61138), a Division of Saint-Gobain Ceramic Materials GmbH. This silica was employed due to its good thermal stability [29]. Millipore Milli-Q® water was employed (18.2 MΩ·cm at 25 °C).

2.2. Catalyst preparation

The P_2O_5-based catalyst was prepared by incipient wetness impregnation using 5 % extra pore volume of the liquid solution using the protocol described in [22]. The silica extrudates were crushed and sieved into a 212–425 μm fraction. Silica (3.0 g) was dried at 150 °C under vacuum for 4 h. After drying, a neoprene stopper was set to prevent water re-adsorption from the air. After the silica was cooled down to room temperature, a H_3PO_4 solution was added. This solution (10 ml) was prepared by mixing a certain amount of H_3PO_4 (Merck, 85 %) with water, resulting in a phosphorous loading of ca. 3 wt% (as P) in the final catalyst. Afterwards, the material was shaken for 4 min at 2500 rpm using a vortexer (VWR DVX-2500) at room temperature and dried at 70 °C overnight in an atmospheric oven. Afterwards, the sample was calcinated at 500 °C for 8 h with a heating rate of 4 °C/min in a Nabertherm P330 muffle furnace.

2.3. Characterisation

2.3.1. ODH-coke

The amount of organic deposit (ODH-coke) in the after-reaction catalyst (i.e., end of the run after 60 h time on stream) was determined by thermogravimetric analysis on a Mettler-Toledo analyzer (TGA/SDTA851e) using a flow of synthetic air of 100 ml/min (STP). The temperature was raised from 30 to 900 °C at 10 °C/min. Physiosorbed water was accounted in the calculation. Temperature programmed oxidation data (TPO) are calculated as −DTGA (i.e., the derivative of the

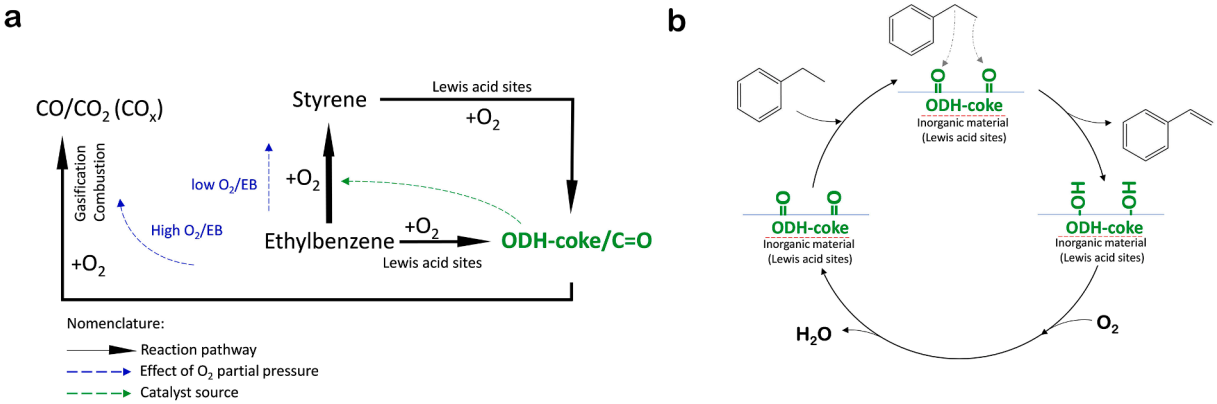

Fig. 1. a) Scheme representing the different reaction pathways in the oxidative dehydrogenation of ethylbenzene into styrene and CO/CO_2 (CO_x) over coked catalysts at industrially-relevant conditions. The ODH-coke is produced via ethylbenzene, styrene, or both, catalysed by Lewis acid sites [9,20]. The styrene active sites are the ketonic (quinone) groups on the ODH-coke. CO_x is assumed to be formed by oxidation/gasification of the ODH-coke [9]. The effect of O_2/EB on selectivity (dashed lines) is based on our prior work [13,14,20–24,28]. The thickness of the lines indicates the reaction rates in qualitative terms. The green dashed line indicates the ODH-coke containing C=O groups being the catalyst for the EB-to-ST step (mechanism is described in b). b) Reaction mechanism for the oxidative styrene synthesis via a quinone-to-hydroquinone redox mechanism [9,28]; these groups are present on the ODH-coke, which is induced by Lewis sites on the inorganic material (i.e., pre-catalyst). The hydroquinone can be restored into quinone via molecular O_2 or activated surface O_2 [16].

TGA).

2.3.2. Gas physisorption

Textural analyses of the fresh and after-reaction catalysts were carried out by N_2 physisorption at −196 °C, on a Micromeritics ASAP 2420 analyser. The fresh catalyst was degassed under vacuum at 300 °C for 10 h. The after-reaction catalyst was degassed at milder conditions, 130 °C for 24 h, to ensure that the ODH-coke was not altered. The surface area was calculated by BET method, S_{BET} and denoted as 'BET area' [30]. The single point total pore volume (V_T) was estimated at a P/P_o of 0.98 in the desorption branch [31]. The pore size distribution was obtained, as an approximation, from the BJH model using the desorption branch. The BJH model, having well-known limitations (e.g. underestimate the pore size) was employed since the available NLDFT models did not provide meaningful results. In the case of the P_2O_5/silica catalysts, the analyses were carried out with Ar at −186 °C. However, this does not change the interpretation.

2.3.3. Acidity assessment

Pyridine acidity measurements were carried out following the procedure and equipment reported elsewhere [20]. The Lewis and Brønsted density values were determined using the correlations reported by Tamura et al. [32] with $\varepsilon = 1.73$ cm/μmol for Lewis acid sites (band at ca. 1438–1456 cm^{-1}) and $\varepsilon = 1.23$ cm/μmol for Brønsted sites (band at ca. 1547–1549 cm^{-1}). The values reported in Table 1 were determined at 150 °C.

2.3.4. Elemental analysis

The Si/Al atomic ratio was determined by quantification of the Si and Al concentrations in solution, after digesting the solid in a HF solution, by inductivity-coupled plasma analysis [33].

2.3.5. Electron microscopy

Transmission electron microscopy (TEM) images were acquired in a JEOL 2100 field emission gun transmission electron microscope at 200 kV, equipped with an EDX spectrometer (Oxford INCA Energy 2000). Before analysis, the material was immersed in ethanol and subsequently deposited onto a holey carbon grid until dryness.

2.4. Catalytic activity

The catalyst tests and reaction product analysis were carried out using the equipment and methods described elsewhere [13,14,20,21]. The tests were carried out at *iso*-volume of the catalyst bed. This is because the design of fixed-bed reactors aims at minimizing the volume to save capital costs. In other words, assessing the catalyst performance per volumetric loading provides a more realistic assessment. The volumetric metrics have been critically highlighted elsewhere for various adsorption-based applications [34–38] and electrochemical energy storage [39,40]. The applied reaction conditions are considered to be industrially relevant. They consist of using a high EB concentration (ca. 10 vol%), limited O_2 and the temperature was chosen high enough to obtain 100 % O_2 conversion. The reaction conditions are given on each graph. The conversions (X) and selectivities (S) are defined as:

$$X_{EB} = \frac{\left[\dot{n}_{EB}\right]_{IN} - \left[\dot{n}_{EB}\right]_{OUT}}{\left[\dot{n}_{EB}\right]_{IN}} \times 100 \quad (1)$$

$$X_{O_2} = \frac{\left[\dot{n}_{O_2}\right]_{IN} - \left[\dot{n}_{O_2}\right]_{OUT}}{\left[\dot{n}_{O_2}\right]_{IN}} \times 100 \quad (2)$$

$$S_{Product\ X} = \frac{\dot{n}_{Product\ X}/p}{\left[\dot{n}_{EB}\right]_{IN} - \left[\dot{n}_{EB}\right]_{OUT}} \times 100 \quad (3)$$

Where the $\dot{n}$-values (mol/h) are the molar flowrates, p is a stoichiometric factor (1 for styrene and 8 for CO_x). The subscript '*EB*' refers to ethylbenzene and *'Product X'* refers to the product which can be styrene or CO_x. The subscript 'IN' means the molar flow entering the reactor, whereas 'OUT' means the flow out of the reactor.

In the discussion, the term activation means that O_2 is fully converted though additional ODH-coke may be deposited. The main detected products were styrene and CO/CO_2 (CO_x). A small fraction of benzene, toluene and short hydrocarbons was observed (ca. 0.8-2.6 % in total, as selectivities), which remained constant at all conditions. Heavier products were also observed but in a much lower concentration. Mass balances were acceptable (>97 %). The difference is mostly coming from the ODH-coke and condensation of heavy byproducts in the lines/valves, which represents a small fraction of the total fed ethylbenzene.

3. Results and discussion

3.1. Aluminosilicate catalyst

The properties of the catalyst will be first briefly discussed and then the catalytic activity; fast-screening and long stability test whose discussion involves a reaction model to explain the results.

3.1.1. Properties of the MSU

The MSU shows an isotherm type IV with H1 hysteresis (Fig. 2a) that corresponds to a pore network with good connectivity [30,41]. The isotherm does not level off at high P/P_o and that implies having an additional type II character due to unfilled macropores [30,37]. The pore size distribution reveals a well-defined maximum located at ca. 13 nm (inset Fig. 2a). The desorption data provide the size of the windows

Table 1
Textural parameters derived from N_2 adsorption at − 196 °C, acidic properties and coke content for the fresh and spent catalysts (n.d. means not determined).

Material	S_{BET} (m^2/g)	V_T (cm^3/g)	Lewis (μmol/g)	Lewis^{bed} [c] (μmol)	Brønsted (μmol/g)	Brønsted^{bed} [c] (μmol)	TGA ODH-coke (wt.%)	S_{BET}^{bed} [d] (m^2)	Strength Lewis [e] (%)
MSU fresh	544	1.982	51	7	11	2	–	79	61
MSU spent [a]	154	0.387	n.d.	n.d.	n.d.	n.d.	60.4	56	n.d.
P_2O_5/silica fresh	161[b]	0.792	62	26	158	66	–	67	79
P_2O_5/silica spent [a]	104[b]	0.262	n.d.	n.d.	n.d.	n.d.	39.1	72	n.d.

a. After-reaction catalyst for the 60-h run.

b. The BET areas were converted into N_2 according to the correlation reported in [41], where $S_{BET}^{N_2} = 1.227 \cdot S_{BET}^{Ar}$.

c. Quantity in the catalyst bed calculated as Lewis^{bed} = W^{bed} (g)·Lewis (μmol/g) and Brønsted^{bed} = W^{bed} (g)·Brønsted (μmol/g), where W^{bed} is the weight of the catalyst in the bed.

d. Quantity in the catalyst bed calculated as $S_{BET}^{bed} = W^{bed}$ (g)·S_{BET} (m^2/g). In the case of the spent catalysts, the weight was corrected by the gain due to the ODH-coke.

e. Strength of Lewis sites as determined by the pyridine350/pyridine150 ratio, where pyridine350 and pyridine150 are the peak area of the PyL bands (pyridines interacting with Lewis sites) on desorption at 350 and 150 °C, respectively. It provides the ratio of pyridine molecules neutralizing Lewis sites that survived desorption at 350 °C with respect to 150 °C as reference point.

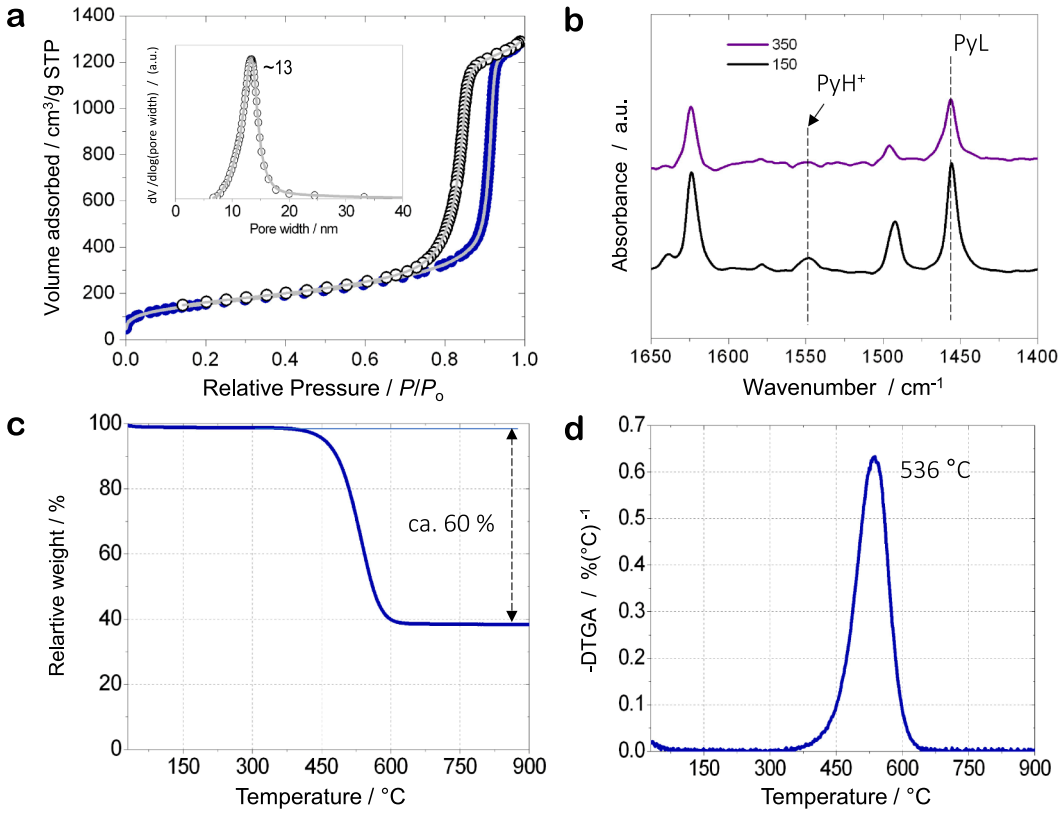

Fig. 2. Aluminosilicate MSU catalyst. a) Nitrogen isotherm of the fresh MSU at −196 °C. The inset corresponds to the BJH pore size distribution of the desorption branch; b) FTIR spectra of the pyridine (Py) vibrations adsorbed on the MSU recorded at various temperatures as indicated in the labels, in degree Celsius. PyH^+ corresponds to Brønsted sites and PyL to Lewis acid sites; c) TGA profile of the spent catalyst and d) TPO profile of the spent catalyst.

connecting larger spherical-like cavities [42]. Therefore, this is the smallest pore size in the structure. TEM images evidence a sponge-type structure of interconnected spherical-like open pores connected by windows (Fig. S1), also known as mesocellular foam molecular sieves. The BET area is 544 m^2/g in agreement with a previous study [37].

The suitability of this aluminosilicate to produce active ODH-coke for styrene synthesis was evaluated by its acidity. In particular, using pyridine adsorption FTIR by looking at the nature and density of the acid sites. The material contains both Brønsted and Lewis acid sites as indicated in Fig. 2b as PyH^+ and PyL, respectively [20]. The spectra were recorded at two degassing temperatures to evaluate the acid strength and this will be discussed later. Quantification of the Lewis acid sites indicate that the material has 51 μmol/g and this corresponds to 7 μmol in the catalyst bed (Table 1). Therefore, Lewis acidity is available to produce ODH-coke. This was later confirmed with the spent catalyst that shows ca. 60 wt% deposited coke (Fig. 2c, Table 1). The MSU also has Brønsted acid sites (Table 1). However, no significant cracking/dealkylation activity were observed during the catalytic tests. Only a small fraction of benzene and toluene was found, ca. 1.6 % as selectivity. Note that this fraction is also observed in the direct dehydrogenation catalyst based on Fe-oxide [7]. Therefore, the MSU's Brønsted acidity does not play a significant role in this reaction but the ODH-coke for the main (styrene) and side reactions (CO_x). The TPO profile shows that the ODH-coke is oxidized with a maximum rate at ca. 536 °C (Fig. 2d). This temperature is lower than for conventional hydrocarbon-based coke [43,44] which oxidizes at temperatures higher than 600 °C (same heating rate and same atmosphere when comparing the TPO profiles). The lower temperature can be related to the high oxygen content in the ODH-coke [9,20], which makes its oxidation/combustion easier than conventional hydrocarbon-derived cokes.

3.1.2. *Fast-screening catalytic test*

First evidence of deactivation was observed by a fast-screening catalytic test (Fig. 3). The catalyst performance was assessed under industrially-relevant reaction conditions. That implies a high EB concentration (ca. 10 vol%) and O_2/EB = 0.6, so oxygen was added under restricted concentration to ensure that it is fully converted. This is an important condition for industrial applicability because unreacted oxygen could create explosive conditions in the purification section of an industrial setting. We also looked at a lower O_2/EB ratio of 0.2 to understand its effect on selectivity.

At the onset of the reaction, the build-up of active ODH-coke occurs and the EB conversion raises sharply (Fig. 3a), a phenomenon that is often denoted as activation [20,22,23,25]. This phenomenon is slower for MSU than for the γ-alumina [20]. It might be correlated to the lower amount of Lewis sites in the bed, 7 μmol (MSU, Table 1) vs 69 μmol in the bed (γ-alumina) [20]. The selectivities to styrene (ST) and CO_x sum up to ca. 100 % as competitive routes; both routes consume O_2 which is limiting. That means that a modification of one (ST or CO_x) leads to a change towards the other (CO_x or ST). In other words, if the CO_x selectivity decreases by x%, the ST selectivity increases by x%, and vice versa. This is seen in Fig. 3b and c; e.g. increased CO_x formation leads to decreased styrene, with time on stream (red dashed lines). Note that the small fraction of benzene/toluene does not affect the trends between ST and CO_x as the fraction was very small and constant along the run. The catalyst performance, as shown in Fig. 3a–c, leads to the conclusion that lower O_2 partial pressure enhances the styrene selectivity (Fig. 3b) as the CO_x pathway is decreased (Fig. 3c). This however has a strong penalty on the EB conversion and ST yield that are both lowered (Fig. 3a and Fig. S2, respectively). This shortcoming can be overcome by operating under an O_2-stage feeding, that maintains a high ST selectivity and the EB conversion is notably improved [22].

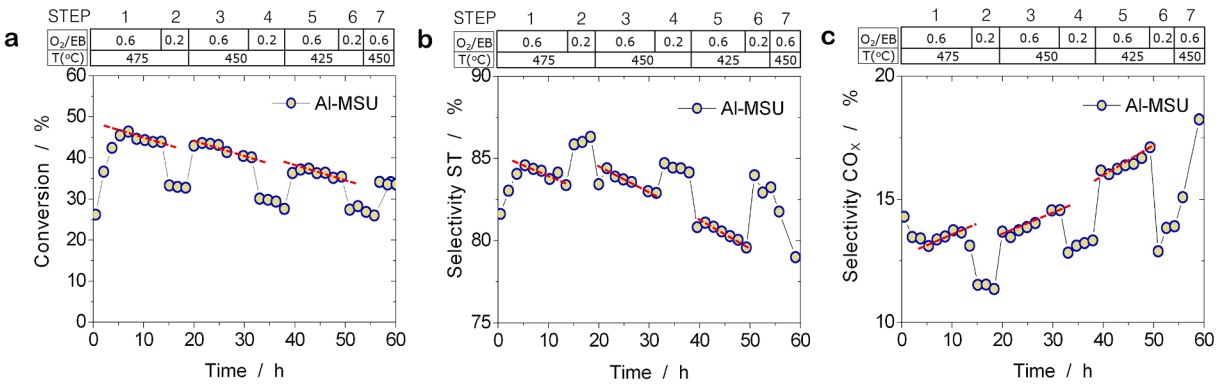

Fig. 3. Aluminosilicate MSU catalyst. Fast-screening test for the oxidative dehydrogenation of ethylbenzene to styrene (ST) and CO_x (side product). Catalyst performance parameters as a function of temperature and O_2/EB: a) ethylbenzene conversion, b) styrene selectivity and c) CO_x selectivity. GHSV = 2700 h^{-1}, 10 vol% EB. The O_2/EB values given in the heading are the values set in the mass-flow controllers for simplicity.

The run shows an important observation in terms of deactivation. The EB conversion drops with time on stream (red dashed lines in Fig. 3a) whilst the CO_x selectivity increases (Fig. 3c). The decreasing ST selectivity (Fig. 3b) results from both product routes competing for the limited O_2. Thus, a change in one of the selectivities has a reversed effect on the other. These observations are in line with previous studies at the same reaction conditions [20,22]. To gain more insight on this deactivation pattern, we carried out a longer catalyst test at isothermal conditions, which will be discussed with a formal reaction model.

3.1.3. *Long stability and reaction model analysis*

A longer stability test shows the typical activation where the EB conversion reaches a maximum (Fig. 4a). This activation takes longer than in Fig. 3a due to the lower temperature. After the maximum, the conversion decays slowly with time on stream. One hypothesis is that the EB's decay is due to the plugging of the catalyst by deposition of ODH-coke. Fig. S3 shows the isotherm of the spent catalyst and the decreased textural parameters are provided in Table 1. However, previous studies showed that surface area does not play a positive role at these reaction conditions; aluminas with decreasing surface areas (per bed) showed in fact higher EB conversions [20,28]. Regarding plugging itself, for the optimal catalyst in Zarubina et al. [20], the BET area in the bed increased after coking (58 vs 78 m^2 in the bed, with slightly smaller mesopores) and deactivation was observed [20]. Therefore, we looked at another hypothesis, whether the EB conversion is linked to the selectivity.

In a previous study, a reaction model correlating conversion and selectivity was developed for this reaction [28]. The model is obtained by setting an O_2 mass balance across the reactor, considering the main (4) and side reactions (5,6):

$$R1 \quad C_8H_{10} + \frac{1}{2}\,O_2 \rightarrow C_8H_8 + H_2O \tag{4}$$

$$R2 \quad C_8H_{10} + \frac{13}{2}O_2 \rightarrow 8CO + 5H_2O \tag{5}$$

$$R3 \quad C_8H_{10} + \frac{21}{2}O_2 \rightarrow 8CO_2 + 5H_2O \tag{6}$$

The procedure to develop the reaction model equation can be found in the Appendix, resulting in the following expression:

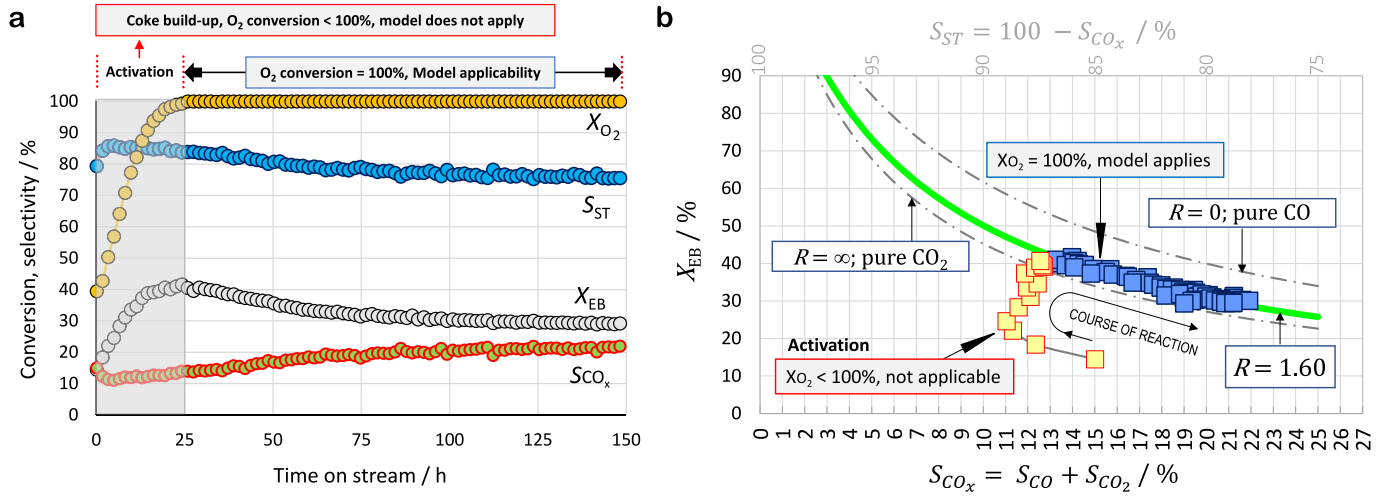

Fig. 4. Aluminosilicate MSU catalyst. **a)** Stability test at 450 °C, GHSV = 2700 h^{-1}, 10 vol% EB, O_2/EB = 0.6 (mass flow controller value). Parameters: EB conversion (X_{EB}), selectivity to styrene (S_{ST}), selectivity to CO_x (S_{CO_x}) and O_2 conversion (X_{O_2}). The graph indicates where the model applies, i.e., at full O_2 conversion. **b)** Reaction model representation of the EB conversion (X_{EB}) as a function of the selectivity to CO_x (S_{CO_x}), including experimental data points. Model parameters: $\left(\left[\dot{n}_{O_2}\right]/\left[\dot{n}_{EB}\right]\right)_{IN}^{\text{mass balance}} = 0.67$, $R = 1.60$. These parameters are average values obtained from the experimental data. The graph also includes the theoretical curves when CO_x is either pure CO or pure CO_2 as points of comparison, i.e., the lowest and highest boundaries in the model with respect to CO_x.

$$X_{EB}(\%) = \frac{\left(\left[\dot{n}_{O_2}\right] \Big/ \left[\dot{n}_{EB}\right]\right)_{\text{IN}}^{\text{mass balance}} \cdot 10^4}{\frac{1}{2}S_{ST} + \frac{13}{2}S_{CO} + \frac{21}{2}S_{CO_2}} = \frac{\left(\left[\dot{n}_{O_2}\right] \Big/ \left[\dot{n}_{EB}\right]\right)_{\text{IN}}^{\text{mass balance}} \cdot 10^4}{\frac{1}{2}(100 - S_{CO_x}) + \frac{13}{2}\left(\frac{1}{R+1}S_{CO_x}\right) + \frac{21}{2}\left(\frac{R}{R+1}S_{CO_x}\right)} \quad (7)$$

and

$$S_{ST} + S_{CO} + S_{CO_2} = S_{ST} + S_{CO_x} = 100 \quad (8)$$

Where $\left(\left[\dot{n}_{O_2}\right] \Big/ \left[\dot{n}_{EB}\right]\right)_{\text{IN}}^{\text{mass balance}}$ can be determined experimentally by a mass balance of the detected compounds and R is the ratio between CO_2 and CO. We employed this value, $\left(\left[\dot{n}_{O_2}\right] \Big/ \left[\dot{n}_{EB}\right]\right)_{\text{IN}}^{\text{mass balance}}$, because there can be discrepancies between instruments (mass-flow controllers and gas analysis). Using the same instrument (gas analysis) brings more accuracy.

The model explains that in a system of competing reactions having a limiting reactant (O_2 in this system), the conversion of the other reactant (ethylbenzene) is not an independent variable but dependent on the selectivity of the competing reactions. Consequently, the conversion of the reactant present in excess and the selectivities are linked. The model was originally applied to understand the performance of aluminas to explain the enhanced EB conversion under steady-state operation [28].

The reaction model line was calculated at the reaction conditions and is represented in Fig. 4b together with the experimental data. During the activation period, the O_2 conversion is below 100 % (Fig. 4a) and the model is not applicable. This is clearly seen in Fig. 4b where the experimental data deviate in this period (yellow squares). When oxygen reaches 100 % conversion, the model applies. The experimental data nicely fit the model (Fig. 4b). The whole course of the reaction is shown to highlight how the reaction evolves with time on stream. The goodness of the model fitting was quantified by statistical analysis and shows a low relative standard deviation of 2.5 % (Fig. 5a). In addition, the data scatter around the model line and there are no strange data artifacts as seen in the residual graph (Fig. 5b).

As a consequence, this reaction model analysis proves that the decay in the EB conversion with time on stream is due to the catalyst becoming more selective to CO_x and less to styrene. Therefore, rather than having two deactivating parameters, conversion and selectivity, there is a single aspect associated to the catalyst stability: the selectivity. As both product routes compete, we cannot discriminate which one is the dominating factor; the catalyst being more selective to CO_x or less to ST (or even both). In other words, in a situation when the catalyst becomes more selective to CO_x, it consumes the O_2 intended for the styrene synthesis. But on the other way, if the catalyst becomes less selective to styrene, the exceeding O_2 is employed in the CO_x-forming reactions.

A more accurate model could be developed considering the small selectivities to benzene, toluene and short hydrocarbons, which was ca. 2.6 % and it remained a constant value in the whole test (Fig. 6). In the appendix, the model is further expanded for this case considering that these byproducts are formed either from ethylbenzene or styrene. If these compounds originate from ethylbenzene, they do not consume O_2, and the modification of the model will result in:

$$X_{EB}(\%) = \frac{\left(\left[\dot{n}_{O_2}\right] \Big/ \left[\dot{n}_{EB}\right]\right)_{\text{IN}}^{\text{mass balance}} \cdot 10^4}{\frac{1}{2}(100 - S_{Others} - S_{CO_x}) + \frac{13}{2}\left(\frac{1}{R+1}S_{CO_x}\right) + \frac{21}{2}\left(\frac{R}{R+1}S_{CO_x}\right)} \quad (9)$$

and

$$S_{ST} + S_{CO_x} + S_{Others} = 100 \quad (10)$$

Where S_{Others} correspond to benzene, toluene and short hydrocarbons.

If these byproducts originate from styrene, the reactions do not consume O_2 but the formation of styrene does. The model needs to be adjusted to this situation, see appendix, resulting in:

$$X_{EB}(\%) = \frac{\left(\left[\dot{n}_{O_2}\right] \Big/ \left[\dot{n}_{EB}\right]\right)_{\text{IN}}^{\text{mass balance}} \cdot 10^4}{\frac{1}{2}(100 - S_{Short\,HC} - S_{CO_x}) + \frac{13}{2}\left(\frac{1}{R+1}S_{CO_x}\right) + \frac{21}{2}\left(\frac{R}{R+1}S_{CO_x}\right)} \quad (11)$$

and

$$S_{ST} + \overbrace{S_{Benzene} + S_{Toluene} + S_{Short\,HC}}^{S_{Others}} + S_{CO_x} = 100 \quad (12)$$

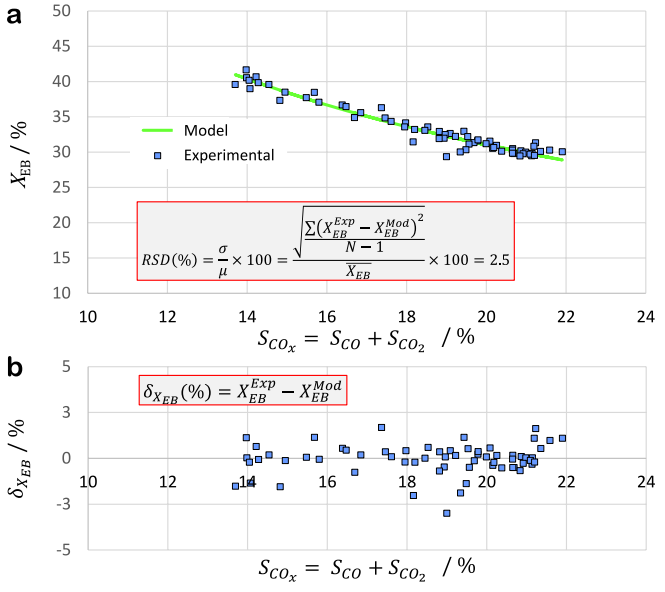

Fig. 5. Aluminosilicate MSU catalyst. Statistical data analysis where model applies in Fig. 4b. a) model fitting and relative standard deviation, RSD (σ is the standard deviation and μ is the mean value), b) residuals. X_{EB}^{Exp} are the experimental data, X_{EB}^{Mod} are the values calculated from the model (see model parameters in Fig. 4b), $\overline{X_{EB}}$ is the average EB conversion in the whole period and N is the number of data points.

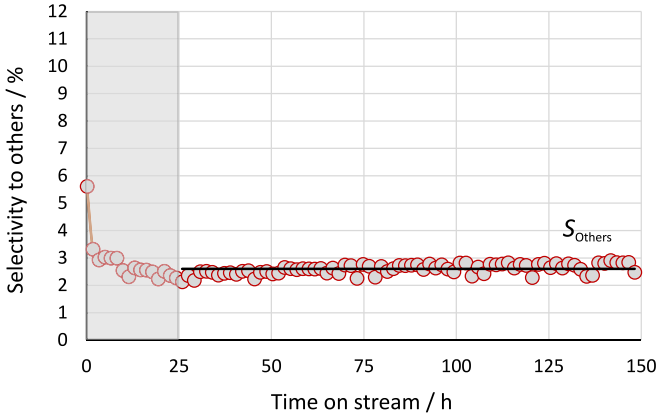

Fig. 6. Aluminosilicate MSU catalyst. Selectivity to others (i.e., benzene, toluene and short hydrocarbons) with time on stream. Reaction conditions are given in Fig. 4. The straight line indicates the average value in the model region, S_{Others} = 2.6 %. The dashed area corresponds to the activation period with a slightly higher selectivity to these byproducts. The concentration of short hydrocarbons was ca. 1 % (not shown).

The model equation lines were calculated for these two situations and compared to a byproducts-free case from Fig. 4b, in Fig. 7. The results are nearly identical to the case assuming it to be zero. Therefore, the assumption that CO_x and ST sum up to ca. 100 % (Eqs. (7) and (8)) provides accurate data.

For the sake of completeness, the data from Fig. 3 also fits the reaction model (Fig. 8).

3.2. P_2O_5/silica catalyst

Another reference catalyst, P_2O_5/silica, was investigated regarding its deactivation. Note that a comparison between both materials in this study regarding their different selectivities is out of the scope of this work.

3.2.1. Properties of the P_2O_5/silica

The catalyst was prepared by incipient wetness impregnation using H_3PO_4 as precursor followed by controlled drying and calcination, with a concentration of ca. 3 wt% as P. The material has a mesoporous nature with an isotherm type IV with H1 hysteresis (Fig. 9a). The isotherm is very similar to that of the MSU and the same interpretation is valid here. The pore size is larger and centred at 17 nm; its distribution is broader than the MSU (inset Fig. 9a). Despite the comparable isotherm, the MSU is much lighter than the P_2O_5/silica. In other words, more P_2O_5/silica catalyst weight was loaded in the reactor, where the tests were carried out at *iso*-volume. The BET area is lower than the MSU (Table 1) but the BET area in the bed is comparable due to the differences in the bulk densities. For this material, the Lewis acidity necessary to promote the ODH-coke mainly arises from the P_2O_5, as the silica itself has very low acidity (Fig. 9b). The quantified Lewis acidity is 62 µmol/g, or 26 µmol in the bed (Table 1), suitable to produce ODH-coke. The amount of deposited ODH-coke for a 60 h-run was ca. 39 wt% (Fig. 9c, Table 1), which is lower than the MSU. This is likely due to the lower pore volume so it can accommodate less ODH-coke per mass. The TPO decomposition is a single process, centred at ca. 563 °C (Fig. 9d). This catalyst has more Brønsted sites than MSU (Table 1), but no cracking activity was observed. The selectivity to benzene and toluene was smaller than for MSU and below 1 %.

3.2.2. Fast-screening catalytic test

The fast-screening test shows comparable deactivation trends as those found for MSU in terms of EB conversion and ST/CO_x selectivities (Fig. S4). This catalyst is more selective towards ST and less to CO_x compared to the MSU and in general for aluminas [20]. The selectivity to byproducts is smaller and below 1 % (Fig. S4d).

3.2.3. Long stability and reaction model analysis

The long-stability performance for this type of catalyst is similar to the MSU (Fig. 10a). The Lewis acidity promotes the deposition of ODH-coke and the EB conversion increases until reaching the point at which O_2 is fully converted. After this point, the EB conversion and the ST selectivity decrease, whereas the CO_x selectivity increases. In this test, we carried out three consecutive runs with two intermediate reactivations. In the reactivation the EB feed is switched off; in this way O_2 combusts/gasifies the ODH-coke and the reactivation is completed when O_2 conversion reaches zero. The catalyst performance for each run is nearly identical to each other, showing good reproducibility and stability against reactivation of the catalyst.

Application of the reaction model (Eq. (7)) to the experimental data is shown in Fig. 10b, where the three runs are plotted comparatively. Some data points are not fitting the model line as these points correspond to O_2 conversion below 100 %, where the model does not apply.

The goodness of the fitting can be found in Fig. 11 for each separate run. The relative standard deviation is low with values of 2.5, 2.5 and 4.6 %. The latter is due to the larger data scattering in the test (see Fig. 10a, run 3), associated to the slightly higher error in the analysis system due to tar condensation in the sampling system that requires cleaning. For the three runs, the data scatter around the model line as indicated in the residual graphs. In general, the reaction model fits very well the experimental data. These results confirm the deactivation behaviour of the MSU catalyst, as described in the previous section.

3.3. Further discussion

The changes in catalyst selectivity remain an open topic, though

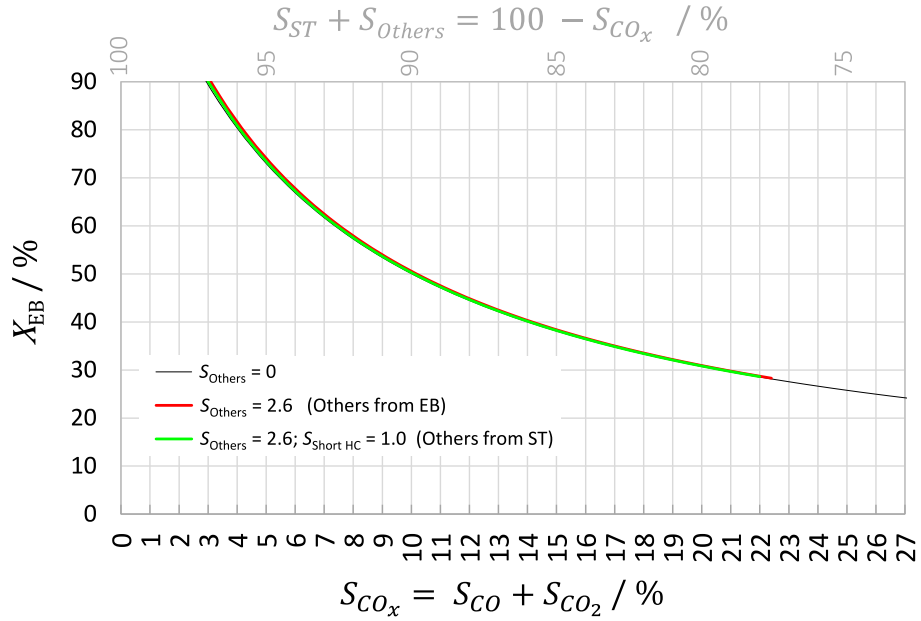

Fig. 7. Reaction model representation of the EB conversion (X_{EB}) as a function of the selectivity to CO_x (S_{CO_x}). Model parameters: $\left(\left[\dot{n}_{O_2}\right]/\left[\dot{n}_{EB}\right]\right)_{IN}^{\text{mass balance}} = 0.67$, $R = 1.60$. Considering three cases as indicated in the graph. Note that in this case $S_{ST} + S_{CO_x} + S_{Others} = 100$ %, where $S_{Others} = S_{Benzene} + S_{Toluene} + S_{Short\ HC}$. $S_{Others} = 2.6$ % and $S_{Short\ HC} = 1.0$ % are based on experimental data. The corresponding model equations can be found in the main text and the derivations in the Appendix.

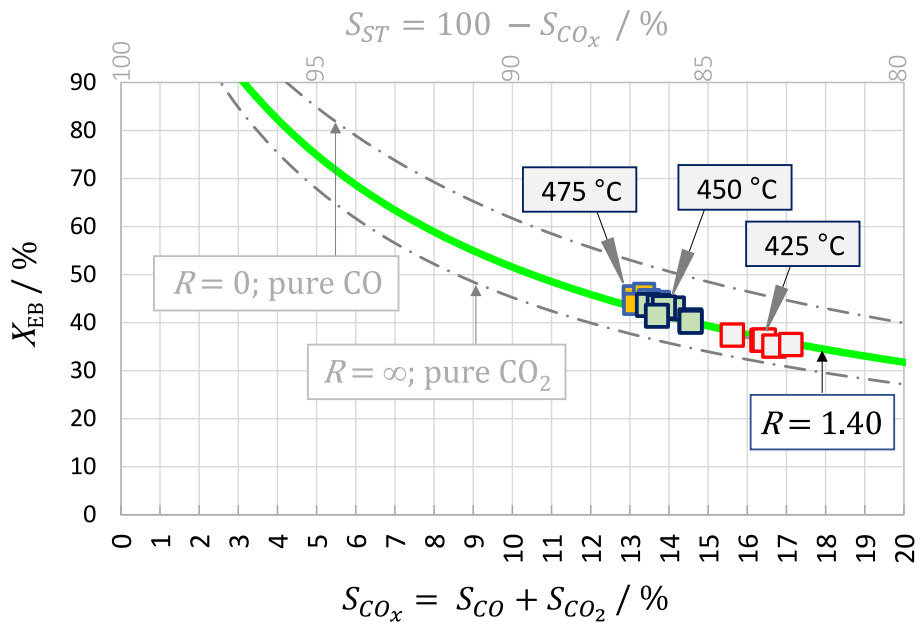

Fig. 8. Aluminosilicate MSU catalyst. Reaction model representation of the EB conversion (X_{EB}) as a function of the selectivity to CO_x (S_{CO_x}), including experimental data points from Fig. 3 (steps 1, 3 and 5, at $X_{O_2} = 100\%$). Model parameters: $\left(\left[\dot{n}_{O_2}\right]/\left[\dot{n}_{EB}\right]\right)_{IN}^{\text{mass balance}} = 0.68$, $R = 1.40$. These parameters are average values obtained from the experimental data. The graph includes the theoretical curves when CO_x is either pure CO or pure CO_2 as points of comparison, i.e., the lowest and highest boundaries in the model with respect to CO_x.

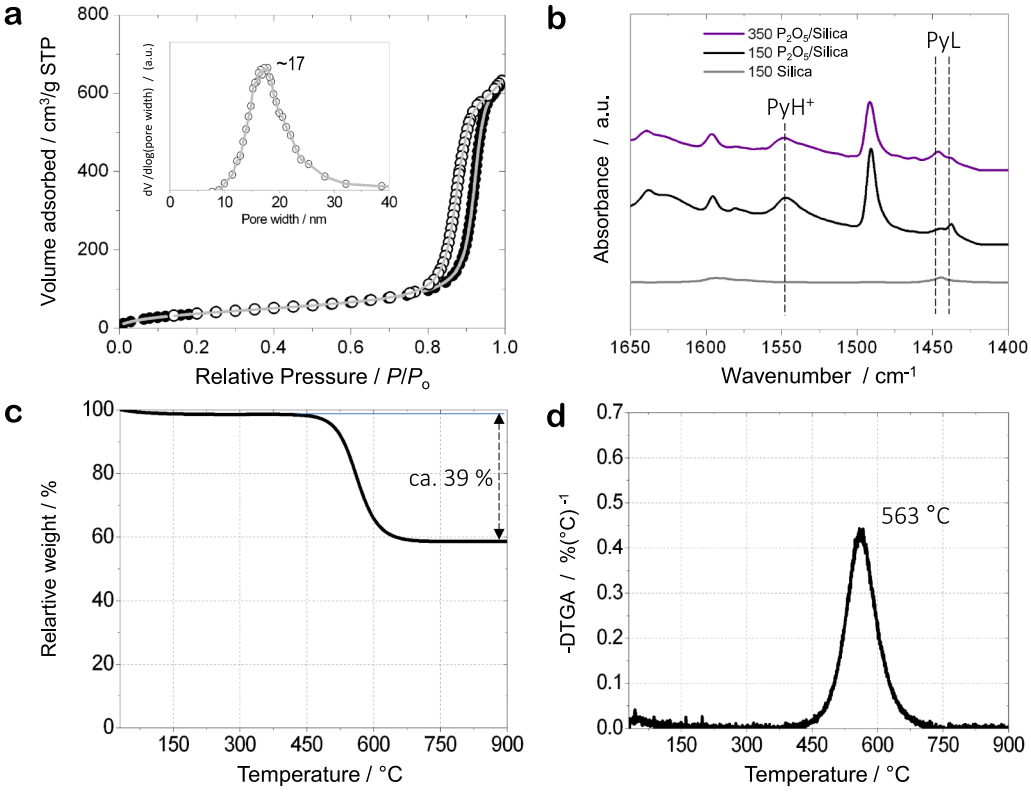

Fig. 9. P_2O_5/silica catalyst. a) Argon isotherm of the fresh material at −186 °C. The inset corresponds to the BJH pore size distribution of the desorption branch; b) FTIR spectra of the pyridine (Py) vibrations adsorbed on the fresh catalyst recorded at various temperatures as indicated in the labels, in degree Celsius. PyH^+ corresponds to Brønsted sites and PyL to Lewis acid sites. The bare silica was included for comparison.; c) TGA profile of the spent catalyst and d) TPO profile of the spent catalyst.

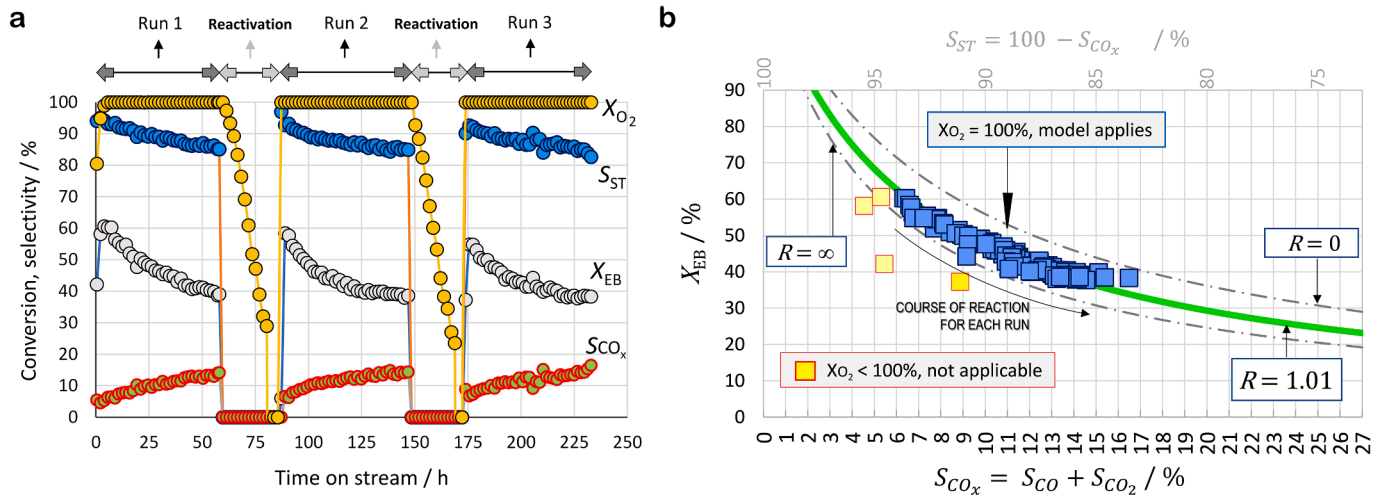

Fig. 10. P_2O_5/silica catalyst. a) Stability test at 500 °C, GHSV = 2700 h^{-1}, 10 vol% EB, O_2/EB = 0.6 (mass flow controller value). Parameters: EB conversion (X_{EB}), selectivity to styrene (S_{ST}), selectivity to CO_x (S_{CO_x}) and O_2 conversion (X_{O_2}). The graph indicates two intermediate reactivation steps; the CO_x profiles have been omitted for these periods since CO_x comes from the combustion/gasification of the ODH-coke. The O_2 conversion is plotted to show when the ODH-coke is fully removed, when $X_{O_2} = 0$. b) Reaction model representation of the EB conversion (X_{EB}) as a function of the selectivity to CO_x (S_{CO_x}), including experimental data points. Model parameters: $\left(\left[\dot{n}_{O_2}\right]/\left[\dot{n}_{EB}\right]\right)^{\text{mass balance}}_{\text{IN}} = 0.63$, $R = 1.01$. These parameters are average values obtained from the experimental data. The graph also includes the theoretical curves when CO_x is either pure CO or pure CO_2 as points of comparison, i.e., the lowest and highest boundaries in the model with respect to CO_x.

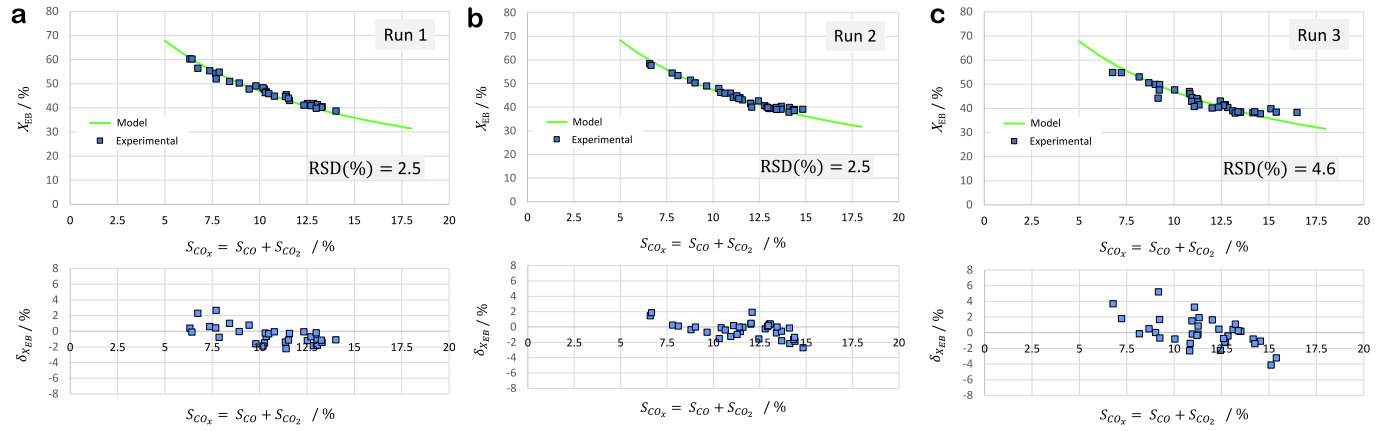

Fig. 11. P_2O_5/silica catalyst. Statistical data analysis where model applies in Fig. 10b; top) model fitting and relative standard deviation (RSD), bottom) residuals: a) Run 1, b) Run 2) and c) Run 3. See model parameters in Fig. 10b.

some suggestions can be outlined. The nature of the ODH-coke (i.e., concentration of active sites, C=O groups in close proximity [9,16,18,19]) determines its styrene selectivity and this can be changing during the reaction. The sites/conditions responsible for the CO_x formation need to be understood. These sites have not been reported in the literature and can be as crucial as the styrene sites. Another aspect can be the plugging of the pores, so the pore size decreases and diffusional limitations may promote the CO_x-forming reactions. A preferential O_2 diffusion (O_2 being smaller than EB) in plugged pores can increase the local O_2 partial pressure and a higher O_2/EB ratio would be obtained in the plugged pores. This condition enhances the CO_x and decreases the ST selectivities. The effect of the O_2 partial pressures was seen here (Fig. 3 and Fig. S4) and in previous studies [13,14,20–23,28], by manipulating the feedstock composition; the reaction order in O_2 for the CO_x-forming reactions is higher than for styrene. Thus, higher O_2 partial pressures promote the CO_x-forming reactions. That means that an O_2-enrichment in plugged pores favouring CO_x can be a way to explain this. The porosity of the spent MSU (Fig. S3 and Table 1) and P_2O_5/silica (Fig. S5 and Table 1) evidence the depletion of the textural features due to coking. Understanding how both catalysts' porosity changes with coking can be very informative to interpret the selectivity changes, in addition to estimating the diffusivity of EB, ST and O_2.

Concerning the coking, it is noteworthy that the MSU and P_2O_5/silica produced more coke than the γ-alumina (60, 39 vs 30 wt%, Table 1 and [20] at the same reactions conditions and time). This can be related to the higher acid strength of the Lewis sites (61 and 79 % Table 1 vs 35 % for the γ-alumina [20]). Hence, the pore structures of MSU and P_2O_5/silica can be more affected during the reaction by coking.

Overall, several aspects remain open to understand the selectivity changes. The proposed reaction model has already simplified the understanding notably.

4. Conclusions

The oxidative dehydrogenation of ethylbenzene (EB) into styrene over two reference catalysts, under industrially-relevant conditions, shows an activation period in which the EB conversion increases and reaches a maximum. This is attributed to the formation of active ODH-

coke, which acts as catalyst. After that period, O_2 is fully converted and a complex deactivation occurs. The EB conversion drops alongside the styrene selectivity whereas the selectivity to CO_x increases (byproduct). A quantitative reaction model, that was developed under the criterion of full O_2 conversion, reveals that the change in EB conversion is the consequence of the catalyst changing its selectivity; becoming more selective to CO_x and less to styrene. As both routes compete for O_2, we cannot discriminate which one is the ultimate factor affecting the deactivation; the catalyst producing more CO_x or less styrene, or both. Importantly, the model simplifies the understanding of this complex deactivation. Rather than having two downsides (conversion and selectivity), the deactivating parameter is the selectivity, whereas EB conversion is a dependent parameter. Such a dependency selectivity-conversion in catalyst deactivation is a novel concept.

CRediT authorship contribution statement

Ignacio Melián-Cabrera: Writing – original draft, Resources, Project administration, Investigation, Funding acquisition, Formal analysis, Data curation, Conceptualization. **Valeriya Zarubina:** Writing – review & editing, Investigation, Data curation. **Harrie Jansma:** Writing – review & editing, Resources, Investigation, Data curation.

Declaration of competing interest

The authors declare that they have no known competing financial interests or personal relationships that could have appeared to influence the work reported in this paper.

Data availability

Data will be made available on request.

Acknowledgements

This research was supported by the Dutch Technology Foundation STW (STW07983), a division of the Netherlands Organization for Scientific Research (NWO). The project was experimentally carried out at Groningen University and Delft University of Technology. The work was completed (data curation and writing) by I.M.C. at La Laguna University. Prof.Em. M. Makkee and Dr. C. Nederlof are thanked for their contributions in the STW project. Dr. M.C. Capel Sánchez (Spanish National Research Council) is thanked for her assistance in the TEM analysis. Ing. B. van der Linden is thanked for carrying out the FTIR measurements. This work is dedicated to Prof. Bárbara T. García Pawelec, for her recent appointment as ad honorem senior scientist at the Spanish National Research Council, which is self-speaking of her brilliant career and dedication.

Appendix

In this section, supplemental information about the reaction model is provided. The following equation represents the O_2 mass balance for the reactions R1, R2 and R3 (reactions are given in the main text):

$$\left[\dot{n}_{O_2}\right]_{\mathrm{IN}} = \left[\dot{n}_{O_2^{R1}} + \dot{n}_{O_2^{R2}} + \dot{n}_{O_2^{R3}}\right]_{\mathrm{consumed}} \tag{A1}$$

Eq. (A1) means that all O_2 is consumed in the reactions R1, R2 and R3, where:

$$\dot{n}_{O_2^{R1}} = \frac{1}{2}\dot{n}_{ST} \tag{A2}$$

$$\dot{n}_{O_2^{R2}} = \frac{13/2}{8}\dot{n}_{CO} \tag{A3}$$

$$\dot{n}_{O_2^{R3}} = \frac{21/2}{8}\dot{n}_{CO_2} \tag{A4}$$

$$X_{EB} = \frac{\left[\dot{n}_{EB}\right]_{\mathrm{IN}} - \left[\dot{n}_{EB}\right]_{\mathrm{OUT}}}{\left[\dot{n}_{EB}\right]_{\mathrm{IN}}} \times 100 \tag{A5}$$

$$S_{ST} = \frac{\dot{n}_{ST}}{\left[\dot{n}_{EB}\right]_{\mathrm{IN}} - \left[\dot{n}_{EB}\right]_{\mathrm{OUT}}} \times 100 \tag{A6}$$

$$S_{CO} = \frac{\dot{n}_{CO}/8}{\left[\dot{n}_{EB}\right]_{\mathrm{IN}} - \left[\dot{n}_{EB}\right]_{\mathrm{OUT}}} \times 100 \tag{A7}$$

$$S_{CO_2} = \frac{\dot{n}_{CO_2}/8}{\left[\dot{n}_{EB}\right]_{\mathrm{IN}} - \left[\dot{n}_{EB}\right]_{\mathrm{OUT}}} \times 100 \tag{A8}$$

For the case of styrene, from Eq. (A6):

$$\dot{n}_{ST} = 0.01 \cdot S_{ST} \cdot \left(\left[\dot{n}_{EB} \right]_{IN} - \left[\dot{n}_{EB} \right]_{OUT} \right) \tag{A9}$$

And from Eq. (A5):

$$\left[\dot{n}_{EB} \right]_{IN} - \left[\dot{n}_{EB} \right]_{OUT} = 0.01 \cdot \left[\dot{n}_{EB} \right]_{IN} \cdot X_{EB} \tag{A10}$$

Introducing Eq. (A10) into A9, it results:

$$\dot{n}_{ST} = 10^{-4} \cdot S_{ST} \cdot \left[\dot{n}_{EB} \right]_{IN} \cdot X_{EB} \tag{A11}$$

From Eqs. (A2) and (A11), the O_2 consumed in reaction (1) can be obtained:

$$\dot{n}_{O_2^{R_1}} = \frac{1}{2} \dot{n}_{ST} = \frac{1}{2} \cdot 10^{-4} \cdot S_{ST} \cdot \left[\dot{n}_{EB} \right]_{IN} \cdot X_{EB} \tag{A12}$$

The same procedure can be done for CO (reaction (2)), resulting in:

$$\dot{n}_{O_2^{R_2}} = \frac{13/2}{8} \dot{n}_{CO} = \frac{13}{2} \cdot 10^{-4} \cdot S_{CO} \cdot \left[\dot{n}_{EB} \right]_{IN} \cdot X_{EB} \tag{A13}$$

The same procedure can be done for CO_2 (reaction (3)), resulting in:

$$\dot{n}_{O_2^{R_3}} = \frac{21/2}{8} \dot{n}_{CO_2} = \frac{21}{2} \cdot 10^{-4} \cdot S_{CO_2} \cdot \left[\dot{n}_{EB} \right]_{IN} \cdot X_{EB} \tag{A14}$$

Eqs. (A12), (A13) and (A14) are introduced in Eq. (A1), from which X_{EB} can be obtained as:

$$X_{EB}(\%) = \frac{\left(\left[\dot{n}_{O_2} \right] / \left[\dot{n}_{EB} \right] \right)_{IN} \cdot 10^4}{\frac{1}{2} S_{ST} + \frac{13}{2} S_{CO} + \frac{21}{2} S_{CO_2}} \tag{A15}$$

It is suggested to use the mass balance values for $\left(\left[\dot{n}_{O_2} \right] / \left[\dot{n}_{EB} \right] \right)_{IN}$ because of accuracy issues between instruments. So having all the values from gas analysis is the most accurate way, and Eq. (A15) transforms as:

$$X_{EB}(\%) = \frac{\left(\left[\dot{n}_{O_2} \right] / \left[\dot{n}_{EB} \right] \right)_{IN}^{\text{mass balance}} \cdot 10^4}{\frac{1}{2} S_{ST} + \frac{13}{2} S_{CO} + \frac{21}{2} S_{CO_2}} \tag{A16}$$

By introducing the R parameter,

$$R = \frac{\dot{n}_{CO_2}}{\dot{n}_{CO}} = \frac{S_{CO_2}}{S_{CO}} \tag{A17}$$

this equation transforms into:

$$X_{EB}(\%) = \frac{\left(\left[\dot{n}_{O_2} \right] / \left[\dot{n}_{EB} \right] \right)_{IN}^{\text{mass balance}} \cdot 10^4}{\frac{1}{2}(100 - S_{CO_x}) + \frac{13}{2} \left(\frac{1}{R+1} S_{CO_x} \right) + \frac{21}{2} \left(\frac{R}{R+1} S_{CO_x} \right)} \tag{A18}$$

and,

$$S_{ST} + S_{CO} + S_{CO_2} = S_{ST} + S_{CO_x} = 100 \tag{A19}$$

These model Eqs. (A18) and (A19) are applicable when there are no additional byproducts.

The deposition of ODH-coke, which contains oxygen, was not considered because the formed ODH-coke represents a very small fraction of the total fed ethylbenzene.

A more accurate model can be set considering the selectivities to others i.e., benzene (B), toluene (T) and short-hydrocarbons (short HC). From the literature [7], these byproducts can be formed in a number of reactions as indicated below, from ethylbenzene and styrene:

Reactions forming toluene:

R4 $C_8H_{10} + H_2 \rightarrow C_7H_8 + CH_4$ (A20)

R5 $C_8H_{10} \rightarrow C_7H_8 + H_2 + C$ (A21)

R6 $C_8H_8 \rightarrow C_7H_8 + C$ (A22)

Reactions forming benzene:

R7 $C_8H_{10} + H_2 \rightarrow C_6H_6 + C_2H_6$ (A23)

R8 $C_8H_{10} \rightarrow C_6H_6 + CH_4 + C$ (A24)

R9 $C_8H_8 + H_2 \rightarrow C_6H_6 + CH_4 + C$ (A25)

Hydrogen from direct ethylbenzene dehydrogenation is unlikely to be produced since higher temperatures are required, typically 600 °C [7]. However, some H_2 can be produced from the WGS reaction (R10) or the cracking reaction R5.

R10 $CO + H_2O \rightleftarrows CO_2 + H_2$ (A26)

The WGS reaction does not modify the model as it does not consume O_2. It may affect the *R* parameter that is obtained experimentally. Below, the model is extended to two scenarios; one considering these other byproducts are obtained from EB (R4, R5, R7 and R8) or ST (R6 and R9).

Ethylbenzene as source of other byproducts:

As these reactions do not consume O_2 (R4, R5, R7 and R8), the modification of the (A16) model, considering (A17) as well, will result in:

$$X_{EB}(\%) = \frac{\left(\left[\dot{n}_{O_2}\right] \Big/ \left[\dot{n}_{EB}\right]\right)_{\text{IN}}^{\text{mass balance}} \cdot 10^4}{\frac{1}{2}S_{ST} + \frac{13}{2}S_{CO} + \frac{21}{2}S_{CO_2}} = \frac{\left(\left[\dot{n}_{O_2}\right] \Big/ \left[\dot{n}_{EB}\right]\right)_{\text{IN}}^{\text{mass balance}} \cdot 10^4}{\frac{1}{2}(100 - S_{Others} - S_{CO_x}) + \frac{13}{2}\left(\frac{1}{R+1}S_{CO_x}\right) + \frac{21}{2}\left(\frac{R}{R+1}S_{CO_x}\right)} \tag{A27}$$

and,

$$S_{ST} + S_{CO} + S_{CO_2} + S_{Others} = S_{ST} + S_{CO_x} + S_{Others} = 100 \tag{A28}$$

Where S_{Others} corresponds to benzene, toluene and short hydrocarbons.

Styrene as source of other byproducts:

The reactions R6 and R9 do not consume O_2 but the formation of styrene (R1) does consume O_2. In that case, Eq. (A12) should be modified considering an 'effective styrene selectivity' comprising styrene, benzene and toluene:

$$\dot{n}_{O_2^{R_1}} = \frac{1}{2}\dot{n}_{ST} = \frac{1}{2} \cdot 10^{-4} \cdot S_{ST}^{eff} \cdot \left[\dot{n}_{EB}\right]_{\text{IN}} \cdot X_{EB} \tag{A29}$$

where,

$$S_{ST}^{eff} = S_{ST} + S_{Benzene} + S_{Toluene} \tag{A30}$$

Considering the previous equations and following the same procedure to derive Eq. (A16), the model will result in:

$$X_{EB}(\%) = \frac{\left(\left[\dot{n}_{O_2}\right] \Big/ \left[\dot{n}_{EB}\right]\right)_{\text{IN}}^{\text{mass balance}} \cdot 10^4}{\frac{1}{2}\left(S_{ST}^{eff}\right) + \frac{13}{2}S_{CO} + \frac{21}{2}S_{CO_2}} = \frac{\left(\left[\dot{n}_{O_2}\right] \Big/ \left[\dot{n}_{EB}\right]\right)_{\text{IN}}^{\text{mass balance}} \cdot 10^4}{\frac{1}{2}\left(S_{ST}^{eff}\right) + \frac{13}{2}\left(\frac{1}{R+1}S_{CO_x}\right) + \frac{21}{2}\left(\frac{R}{R+1}S_{CO_x}\right)} \tag{A31}$$

and,

$$S_{ST} + \overbrace{S_{CO} + S_{CO_2}}^{S_{CO_x}} + \overbrace{S_{Benzene} + S_{Toluene} + S_{Short\ HC}}^{S_{Others}} = \overbrace{S_{ST} + S_{Benzene} + S_{Toluene}}^{S_{ST}^{eff}} + S_{Short\ HC} + S_{CO_x} = 100 \tag{A32}$$

where,

$$S_{ST}^{eff} = 100 - S_{Short\ HC} - S_{CO_x} \tag{A33}$$

Introducing (A33) in (A31), it results in:

$$X_{EB}(\%) = \frac{\left(\left[\dot{n}_{O_2}\right] \Big/ \left[\dot{n}_{EB}\right]\right)_{\text{IN}}^{\text{mass balance}} \cdot 10^4}{\frac{1}{2}\left(100 - S_{Short\ HC} - S_{CO_x}\right) + \frac{13}{2}\left(\frac{1}{R+1}S_{CO_x}\right) + \frac{21}{2}\left(\frac{R}{R+1}S_{CO_x}\right)} \tag{A34}$$

In summary, if these other byproducts are obtained from ethylbenzene, Eq. (A27) is valid. If these byproducts originate from styrene, Eq. (A34) should be applied.

Appendix A. Supplementary data

Supplementary data to this article can be found online at https://doi.org/10.1016/j.cej.2024.152348.

References

[1] J.A. Moulijn, A.E. Van Diepen, F. Kapteijn, Catalyst deactivation: Is it predictable? What to do? Appl. Catal. A Gen. 212 (2001) 3–16, https://doi.org/10.1016/S0926-860X(00)00842-5.

[2] I. Melián-Cabrera, Catalytic materials: Concepts to understand the pathway to implementation, Ind. Eng. Chem. Res. 60 (2021) 18545–18559, https://doi.org/10.1021/acs.iecr.1c02681.

[3] P. Forzatti, L. Lietti, Catalyst deactivation, Catal. Today. 52 (1999) 165–181, https://doi.org/10.1016/S0920-5861(99)00074-7.

[4] J.A. Moulijn, A.E. Van Diepen, F. Kapteijn, Deactivation and regeneration, in: G. Ertl, H. Knözinger, F. Schüth, J. Weitkamp (Eds.), Handbook of Heterogeneous Catalysis, Wiley−VCH Verlag GmbH, Weinheim, 2008, Vol. 4, pp 1829-1846.

[5] A.J. Martín, S. Mitchell, C. Mondelli, S. Jaydev, J. Pérez-Ramírez, Unifying views on catalyst deactivation, Nat. Catal. 5 (2022) 854–866, https://doi.org/10.1038/s41929-022-00842-y.

[6] E.T.C. Vogt, D. Fu, B.M. Weckhuysen, Carbon deposit analysis in catalyst deactivation, regeneration, and rejuvenation, Angew. Chemie - Int. Ed. 62 (2023), https://doi.org/10.1002/anie.202300319.

[7] R.A. Meyers, Handbook of Petrochemicals Production Processes, McGraw-Hill, New York, 2005, pp. 11.3–11.34.

[8] F. Cavani, F. Trifirò, Alternative processes for the production of styrene, Appl. Catal. a, Gen. 133 (1995) 219–239, https://doi.org/10.1016/0926-860X(95)00218-9.

[9] A.E. Lisovskii, C. Aharoni, Carbonaceous deposits as catalysts for oxydehydrogenation of alkylbenzenes, Catal. Rev. 36 (1994) 25–74, https://doi.org/10.1080/01614949408013920.

[10] M.F.R. Pereira, J.J.M. Órfão, J.L. Figueiredo, Oxidative dehydrogenation of ethylbenzene on activated carbon catalysts. I. Influence of surface chemical groups, Appl. Catal. A Gen. 184 (1999) 153–160, https://doi.org/10.1016/S0926-860X(99)00124-6.

[11] J. Zhang, D. Su, A. Zhang, D. Wang, R. Schlögl, C. Hébert, Nanocarbon as robust catalyst: Mechanistic insight into carbon-mediated catalysis, Angew. Chemie - Int. Ed. 46 (2007) 7319–7323, https://doi.org/10.1002/anie.200702466.

[12] A. Rinaldi, J. Zhang, B. Frank, D.S. Su, S.B.A. Hamid, R. Schlögl, Oxidative purification of carbon nanotubes and its impact on catalytic performance in oxidative dehydrogenation reactions, ChemSusChem. 3 (2010) 254–260, https://doi.org/10.1002/cssc.200900179.

[13] V. Zarubina, H. Talebi, C. Nederlof, F. Kapteijn, M. Makkee, I. Melián-Cabrera, On the stability of conventional and nano-structured carbon-based catalysts in the oxidative dehydrogenation of ethylbenzene under industrially relevant conditions, Carbon 77 (2014) 329–340, https://doi.org/10.1016/j.carbon.2014.05.036.

[14] V. Zarubina, H. Talebi, H. Jansma, K. Góra-Marek, C. Nederlof, F. Kapteijn, M. Makkee, I. Melián-Cabrera, On the thermal stabilization of carbon-supported SiO_2 catalysts by phosphorus: Evaluation in the oxidative dehydrogenation of ethylbenzene to styrene and a comparison with relevant catalysts, Appl. Catal. A Gen. 514 (2016) 173–181, https://doi.org/10.1016/j.apcata.2016.01.024.

[15] F. Guo, P. Yang, Z. Pan, X.-N. Cao, Z. Xie, X. Wang, Carbon-doped BN nanosheets for the oxidative dehydrogenation of ethylbenzene, Angew. Chemie - Int. Ed. 56 (2017) 8231–8235, https://doi.org/10.1002/anie.201703789.

[16] W. Qi, P. Yan, D.S. Su, Oxidative Dehydrogenation on nanocarbon: Insights into the reaction mechanism and kinetics via in situ experimental methods, Acc. Chem. Res. 51 (2018) 640–648, https://doi.org/10.1021/acs.accounts.7b00475.

[17] L. Feng, Y. Liu, Q. Jiang, W. Liu, K.-H. Wu, H. Ba, C. Pham-Huu, W. Yang, D.S. Su, Nanodiamonds @ N, P co-modified mesoporous carbon supported on macroscopic SiC foam for oxidative dehydrogenation of ethylbenzene, Catal. Today. 357 (2020) 231–239, https://doi.org/10.1016/j.cattod.2019.02.046.

[18] J.J. Mercadal, D. Osadchii, V. Zarubina, M.J. Valero-Romero, I. Melián-Cabrera, Organocatalyst reactivation with improved performance in O_2-mediated styrene synthesis, Mol. Catal. 529 (2022) 112525, https://doi.org/10.1016/j.mcat.2022.112525.

[19] J.J. Mercadal, A. Mayoral, J.L.G. Fierro, E. García-Bordejé, I. Melián-Cabrera, Improved O_2-assisted styrene synthesis by double-function purification of SWCNT catalyst, Chem. Eng. J. 455 (2023) 140723, https://doi.org/10.1016/j.cej.2022.140723.

[20] V. Zarubina, C. Nederlof, B. Van Der Linden, F. Kapteijn, H.J. Heeres, M. Makkee, I. Melián-Cabrera, Making coke a more efficient catalyst in the oxidative dehydrogenation of ethylbenzene using wide-pore transitional aluminas, J. Mol. Catal. A Chem. 381 (2014) 179–187, https://doi.org/10.1016/j.molcata.2013.10.010.

[21] C. Nederlof, V. Zarubina, I. Melián-Cabrera, H.J. Heeres, F. Kapteijn, M. Makkee, Oxidative dehydrogenation of ethylbenzene to styrene over alumina: Effect of calcination, Catal. Sci. Technol. 3 (2013) 519–526, https://doi.org/10.1039/c2cy20490h.

[22] C. Nederlof, V. Zarubina, I.V. Melián-Cabrera, E.H.J. Heeres, F. Kapteijn, M. Makkee, Application of staged O_2 feeding in the oxidative dehydrogenation of ethylbenzene to styrene over Al_2O_3 and P_2O_5/SiO_2 catalysts, Appl. Catal. A Gen. 476 (2014) 204–214, https://doi.org/10.1016/j.apcata.2014.03.002.

[23] I. Melián-Cabrera, V. Zarubina, C. Nederlof, F. Kapteijn, M. Makkee, An in situ reactivation study reveals the supreme stability of γ-alumina for the oxidative dehydrogenation of ethylbenzene to styrene, Catal. Sci. Technol. 8 (2018) 3733–3736, https://doi.org/10.1039/c8cy00748a.

[24] C. Nederlof, P. Vijfhuizen, V. Zarubina, I. Melián-Cabrera, F. Kapteijn, M. Makkee, Coke formation in the oxidative dehydrogenation of ethylbenzene to styrene by TEOM, Catal. Sci. Technol. 4 (2014) 3879–3890, https://doi.org/10.1039/c4cy00498a.

[25] J. Sheng, W.-C. Li, W.-D. Lu, B. Yan, B. Qiu, X.-Q. Gao, R.-P. Zhang, S.-Z. Zhou, A.-H. Lu, Preparation of oxygen reactivity-tuned FeO_x/BN catalyst for selectively oxidative dehydrogenation of ethylbenzene to styrene, Appl. Catal. B Environ. 305 (2022) 121070, https://doi.org/10.1016/j.apcatb.2022.121070.

[26] X. Zhu, Y. Gao, X. Wang, V. Haribal, J. Liu, L.M. Neal, Z. Bao, Z. Wu, H. Wang, F. Li, A tailored multi-functional catalyst for ultra-efficient styrene production under a cyclic redox scheme, Nat. Commun. 12 (2021) 1329, https://doi.org/10.1038/s41467-021-21374-2.

[27] X. Dai, T. Cao, X. Lu, Y. Bai, W. Qi, Tailored Pd/C bifunctional catalysts for styrene production under an ethylbenzene oxidative dehydrogenation assisted direct dehydrogenation scheme, Appl. Catal. B Environ. 324 (2023) 122205, https://doi.org/10.1016/j.apcatb.2022.122205.

[28] I. Melián-Cabrera, V. Zarubina, Selectivity-induced conversion model explaining the coke-catalysed O_2-mediated styrene synthesis over wide-pore aluminas, Mol. Catal. 524 (2022) 112301, https://doi.org/10.1016/j.mcat.2022.112301.

[29] V. Zarubina, I. Melián-Cabrera, On the geometric trajectories of pores during the thermal sintering of relevant catalyst supports, Scr. Mater. 194 (2021) 113679, https://doi.org/10.1016/j.scriptamat.2020.113679.

[30] M. Thommes, K. Kaneko, A.V. Neimark, J.P. Olivier, F. Rodriguez-Reinoso, J. Rouquerol, K.S.W. Sing, Physisorption of gases, with special reference to the evaluation of surface area and pore size distribution (IUPAC Technical Report), Pure Appl. Chem. 87 (2015) 1051–1069, https://doi.org/10.1515/pac-2014-1117.

[31] L.L. Pérez, V. Zarubina, H.J. Heeres, I. Melián-Cabrera, Condensation-enhanced self-assembly as a route to high surface area α-aluminas, Chem. Mater. 25 (2013) 3971–3978, https://doi.org/10.1021/cm401443b.

[32] M. Tamura, K. Shimizu, A. Satsuma, Comprehensive IR study on acid/base properties of metal oxides, Appl. Catal. A Gen. 433–434 (2012) 135–145, https://doi.org/10.1016/j.apcata.2012.05.008.

[33] M.J. Ortiz-Iniesta, I. Melián-Cabrera, Fenton chemistry-based detemplation of an industrially relevant microcrystalline beta zeolite. Optimization and Scaling-up Studies, Microporous Mesoporous Mater. 206 (2015) 58–66, https://doi.org/10.1016/j.micromeso.2014.12.019.

[34] M.F. De Lange, K.J.F.M. Verouden, T.J.H. Vlugt, J. Gascon, F. Kapteijn, Adsorption-driven heat pumps: the potential of metal-organic frameworks, Chem. Rev. 115 (2015) 12205–12250, https://doi.org/10.1021/acs.chemrev.5b00059.

[35] K.V. Kumar, K. Preuss, M.-M. Titirici, F. Rodríguez-Reinoso, Nanoporous materials for the onboard storage of natural gas, Chem. Rev. 117 (2017) 1796–1825, https://doi.org/10.1021/acs.chemrev.6b00505.

[36] X. Liu, X. Wang, F. Kapteijn, Water and metal-organic frameworks: from interaction toward utilization, Chem. Rev. 120 (2020) 8303–8377, https://doi.org/10.1021/acs.chemrev.9b00746.

[37] I. Melián-Cabrera, V. Zarubina, Surface area per volumetric loading and its practical significance, Microporous Mesoporous Mater. 354 (2023) 112549, https://doi.org/10.1016/j.micromeso.2023.112549.

[38] I. Melián-Cabrera, J.J. Mercadal, A. Mayoral, J.L.G. Fierro, On the surface area per volumetric loading: Its pronounced improvement in densely-packed SWCNT by double-function purification, Microporous Mesoporous Mater. 366 (2024) 112940, https://doi.org/10.1016/j.micromeso.2023.112940.

[39] Y. Gogotsi, P. Simon, True performance metrics in electrochemical energy storage, Science 334 (2011) 917–918, https://doi.org/10.1126/science.1213003.

[40] L. Borchardt, M. Oschatz, S. Kaskel, Tailoring porosity in carbon materials for supercapacitor applications, Mater. Horizons. 1 (2014) 157–168, https://doi.org/10.1039/c3mh00112a.
[41] L. López-Pérez, V. Zarubina, I. Melián-Cabrera, The Brunauer–Emmett–Teller model on alumino-silicate mesoporous materials. How far is it from the true surface area? Microporous Mesoporous Mater. 319 (2021) 111065 https://doi.org/10.1016/j.micromeso.2021.111065.
[42] P. Schmidt-Winkel, W.W.L. Jr, P. Yang, D.I. Margolese, J.S. Lettow, J.Y. Ying, G. D. Stucky, Microemulsion templating of siliceous mesostructured cellular foams with well-defined ultralarge mesopores, Chem. Mater. 12 (2000) 686–696, https://doi.org/10.1021/cm991097v.
[43] R. Huirache-Acuña, B. Pawelec, E. Rivera-Muñoz, R. Nava, J. Espino, J.L.G. Fierro, Comparison of the morphology and HDS activity of ternary Co-Mo-W catalysts supported on P-modified SBA-15 and SBA-16 substrates, Appl. Catal. B Environ. 92 (2009) 168–184, https://doi.org/10.1016/j.apcatb.2009.07.012.
[44] T.A. Zepeda, S. Aguirre, Y.I. Galindo-Ortega, A. Solís-Garcia, R.M.N. Yerga, B. Pawelec, J.C. Fierro-Gonzalez, S. Fuentes, Hydrogenation of CO_2 to valuable C_2–C_5 hydrocarbons on Mn-promoted high-surface-area iron catalysts, Catalysts. 13 (2023) 954, https://doi.org/10.3390/catal13060954.